Electron impact dissociative excitation of O_2: 1. Kinetic energy distributions of fast oxygen atoms

O. P. Makarov, I. Kanik, and J. M. Ajello

Jet Propulsion Laboratory, California Institute of Technology, Pasadena, California, USA

Received 6 November 2000; revised 16 August 2001; accepted 6 September 2001; published 25 November 2003.

[1] The kinetic energy distribution of oxygen atoms resulting from electron impact dissociation of O_2 has been measured. A high-resolution vacuum ultraviolet spectrometer was employed for the measurement of the OI(115.2 nm, 130.4 nm, 135.6 nm) fine-structure emission line profiles at 35 eV and 100 eV electron impact energies. The deconvolved line profiles of atomic oxygen reveal the existence of a broad line profile ($\sim$30–40 mÅ full width at half maximum) produced from a combination of dissociative excitation and dissociative ionization excitation processes. The atomic oxygen kinetic energy distributions at 100 eV electron impact energy spans the energy range from 1 to 10 eV, with a peak value near 1 eV. The excitation functions of OI(115.2 nm, 130.4 nm, 135.6 nm) were measured in the vicinity of threshold, from 14 to 50 eV. The PACS classification is 34.80.Gs (electron scattering-molecular dissociation) and 33.50Dq (molecular spectra-fluorescence). *INDEX TERMS:* 6297 Planetology: Solar System Objects: Instruments and techniques; 6060 Planetology: Comets and Small Bodies: Radiation and spectra; 0310 Atmospheric Composition and Structure: Airglow and aurora; 6005 Planetology: Comets and Small Bodies: Atmospheres—composition and chemistry; 6218 Planetology: Solar System Objects: Jovian satellites; *KEYWORDS:* atmospheres of Jovian satellites, analysis of Hubble Space Telescope UV observations, particle precipitation, electron impact dissociation cross sections, high-resolution UV spectroscopy, aurora and airglow of the Earth

Citation: Makarov, O. P., I. Kanik, and J. M. Ajello, Electron impact dissociative excitation of O_2: 1. Kinetic energy distributions of fast oxygen atoms, *J. Geophys. Res.*, *108*(E11), 5125, doi:10.1029/2000JE001422, 2003.

1. Introduction

[2] The study of the atmosphere of planets and their satellites is of fundamental importance in the attempt to understand the structure and state of evolution. One of the ways to gain such knowledge is to study atomic emissions from different gases in the atmosphere of planets and their satellites. Such studies provide valuable information on densities, gas dynamics, etc. One of the gases whose features are present in the emission spectrum is oxygen. The fingerprint of atmospheric oxygen on a planet or satellite in the solar system can be obtained from the FUV airglow spectrum. For example, the emissions of OI(135.6 nm) and OI(130.4 nm) tend to dominate the FUV airglow spectrum on Io [*Ajello et al.*, 1992a, 1992b; *Clarke et al.*, 1994], on Europa [*Hall et al.*, 1995, 1998], and on Ganymede [*Feldman et al.*, 2000; *Hall et al.*, 1998]. These emissions (except for dayglow 130.4 nm) are produced primarily by electron impact from ambient secondary distributions established by the primary electron flux in the aurora or by the solar EUV in the dayglow. Even on Earth, the observed emission intensity in the FUV spectral region from 122 to 200 nm, in both the airglow and the aurora, is composed of mainly atomic oxygen emissions (OI(130.4 nm) at 72–91% and OI(135.6 nm) at 4–15%) [*Torr et al.*, 1995].

0148-0227/03/2000JE001422

[3] Recent observational studies of the tenuous atmospheres of Europa and Ganymede by the Hubble Space Telescope (HST) have shown that the two icy satellites of Jupiter have oxygen-rich atmospheres. It was suggested that any large satellite with a sufficient amount of water vapor would be expected to build up a substantial atmosphere of O_2 [*Yung and McElroy*, 1977; *Kumar and Hunten*, 1982]. Photolysis of water yields molecular hydrogen and oxygen as well as ozone and a number of radicals. The lighter H_2 molecules would escape from these bodies (e.g., Europa and Ganymede) relatively easily, leaving behind an atmosphere rich in oxygen [*Hall et al.*, 1995, 1998], as demonstrated by the two oxygen emission features which are prominent in the FUV airglow spectrum of Europa [*Hall et al.*, 1995, 1998] and Ganymede [*Feldman et al.*, 2000].

[4] The features are the OI(130.4 nm) and OI(135.6 nm) emission lines resulting from the transitions $g^3P \leftarrow {}^{3,5}S^o$, respectively (see Figure 1). For the satellites of the outer planets the spectrum is produced by the simultaneous dissociation and excitation of atmospheric O_2 by magnetospheric electrons which directly impact the surface or are linked to it by an intrinsic magnetic field. The OI emissions from Europa originate from an exospheric gas distribution subjected to electron impact excitation at all latitudes and longitudes [*Hall et al.*, 1998]. The FUV aurora spectra of Ganymede, which are observed at both poles at latitudes above |40|°, indicate the presence of an intrinsic magnetic field such that Jovian magnetic field lines are linked to the

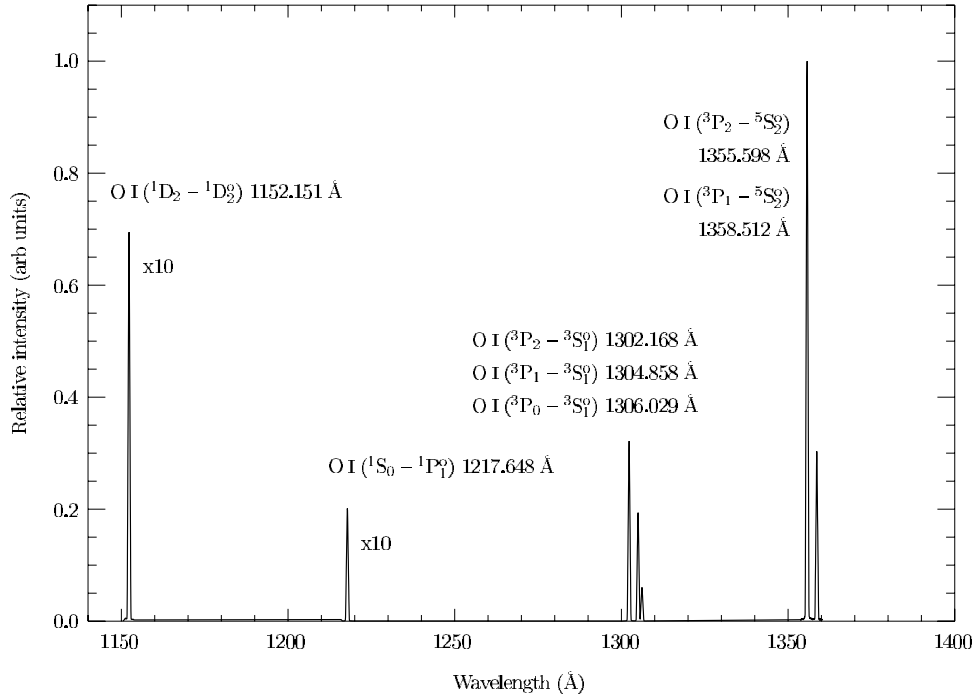

Figure 1. Medium-resolution (0.6 Å full width at half maximum (FWHM)) FUV spectrum of electron impact-induced fluorescence of e + O_2. The four multiplets studied in this study are identified.

surface of Ganymede only at high latitudes [*Feldman et al.*, 2000].

[5] It is well known that the OI(135.6 nm) feature arises from a long-lived transition, with a lifetime of ~180 μs compared to the prompt radiation from the OI(130.4 nm) feature. The analysis of the ratio of the intensities of these two features is paramount in determining the parent species (such as O, O_2, H_2O, CO, SO_2, etc.). Recent measurement of the intensity ratio of the OI(135.6 nm)/OI(130.4 nm) in the airglow of two of Jupiter's satellites, Europa and Ganymede, revealed values of 1.3–2.2 for Europa [*Hall et al.*, 1995, 1998] and 1.6–2.0 for Ganymede [*Feldman et al.*, 2000]. These values indicate that the dominant form of oxygen is molecular rather than atomic. (For atomic oxygen, the ratio calculated on the basis of the electron energy distribution modeled to resemble that near Europa is only ~0.1 [*Hall et al.*, 1995, 1998].)

[6] The prominent OI transitions, primarily the OI (135.6 nm) and OI(130.4 nm) multiplets, resulting from dissociative excitation of O_2, are targeted to obtain accurate absolute excitation function measurements (and consequently, the intensity ratio of OI(135.6 nm)/OI(130.4 nm) over a wide range of electron impact energies) in a two-step investigation. The first part of the investigation, reported here, concerns the measurement of velocity distribution functions of the OI $^5S^o_2$ and OI $^3S^o_1$ atoms released in the dissociative process at 100 eV from the Doppler line profiles of the strong fine-structure lines at 135.56 nm ($g^3P_2 \leftarrow {}^5S^o_2$) and 130.22 nm ($g^3P_2 \leftarrow {}^3S^o_1$), respectively. Also reported is the measurement of the velocity distribution function of the OI $^1D^o_2$ atoms at 1152.15 nm ($^1D_2 \leftarrow {}^1D^o_2$), resulting from dissociative excitation of O_2 at 35 eV and 100 eV electron impact energies. A method has been established to obtain from the Doppler broadening of a given emission line the kinetic energy distribution function of the atoms released in a dissociative process. The method has been utilized in a variety of studies by this group [*Ajello et al.*, 1995a, 1995b, 1996; *Ajello and Ciocca*, 1996; *Ciocca et al.*, 1997; *Beegle et al.*, 1999]. In addition, the optical excitation functions of the OI $g^3P \leftarrow {}^3S^o$ (130.4 nm), OI $g^3P \leftarrow {}^5S^o$ (135.6 nm), and OI $^1D \leftarrow {}^1D^o$ (115.2 nm) transitions produced by electron impact dissociative excitation of O_2 were measured in the threshold region at energies up to 50 eV.

[7] We also completed the measurement of the ratio of the absolute emission cross sections of OI(135.6 nm) and OI(130.4 nm) from electron impact dissociative excitation of O_2 at 100 eV, which is reported in the second part of the investigation by *Kanik et al.* [2003] (hereinafter referred to as Paper 2). The measurements were carried out in a large vacuum chamber with a 1 m optical path. The cylindrically symmetric glow pattern of the optically forbidden OI(135.6 nm) emission about an electron beam with a 0.5 m path length was examined to accurately quantify the total emission intensity for this transition. The total emission intensity was obtained by extrapolating the glow pattern to distances >0.5 m. The extrapolation model was based on the mean energy of fragment atoms obtained in this work and on the recent lifetime values of *Wiese et al.* [1996]. The result of extrapolation was compared to the total intensity of the OI(130.4 nm) prompt radiation. On the basis of the cross section for OI(130.4 nm) by *James et al.* [1988], the absolute emission cross section for OI(135.6 nm) was found to be 6.4×10^{-18} cm^2 at 100 eV (Paper 2).

[8] A brief summary of previous investigations concerning OI emission line profiles and optical excitation cross section measurements at 130.4, 135.6, and 115.2 nm, resulting from dissociative excitation of O_2, is given here. The velocity distribution function of the OI $^3S^o_1$ atoms calculated from the Doppler line profile of the strong fine-structure line at 130.22 nm ($g^3P_2 \leftarrow {}^3S^o_1$), released in the

dissociative excitation of O_2 at 100 eV, is reported here for the first time. The velocity distribution of directly excited OI $^5S^o_2$ atoms and other metastable high-Rydberg fragments have been measured in a time-of-flight measurement by *Freund* [1971]. *Freund* [1971] found a peak kinetic release energy of 1.2 eV per atom in low-energy electron impact studies over the range of 18–60 eV. The only previous measurement of the 115.2 nm line profile was in the study of *Matsumi et al.* [1994]. The velocity distribution of OI $^1D_2$ atoms was determined from the Doppler profile of laser-induced fluorescence of OI ($^1D_2 \leftarrow {}^1D^o_2$) at 115.2 nm. The atoms are generated by the photodissociation of O_2 by linearly polarized light at 157 nm.

[9] In this paper we will briefly describe the experimental apparatus. We will follow with a discussion of the line profile measurements with the 3 m high-resolution spectrometer and the analysis which produces the kinetic energy distribution. The measurements of the excitation function near threshold will be shown. A discussion of the molecular states involved will be based on the threshold behavior of the cross section with energy.

2. Experimental Apparatus

[10] The experimental apparatus has been described in detail elsewhere [*Liu et al.*, 1995; *Ajello et al.*, 1996]. In brief, the apparatus consists of an electron impact collision chamber in tandem with a high-resolution Acton 3.0 m UV spectrometer. The FUV line profiles of atomic oxygen produced by dissociative excitation are measured by crossing a magnetically collimated beam of electrons with a beam of O_2 gas formed by a capillary array at 90°. The impact energy of the electron beam was kept fixed at either 35 eV or 100 eV during line profile measurements. A resolving power of 46,000 (34,000) is achieved by operating the spectrometer in third (second) order. The maximum allowable grating rotation angle of 8° allowed the study in third order of only the line profile of 1152.15 Å ($^1D_2 \leftarrow {}^1D^o_2$) fine structure. The 1302.17 Å ($g^3P_2 \leftarrow {}^3S^o_1$) and 1355.60 Å ($g^3P_2 \leftarrow {}^5S^o_2$) fine-structure lines were studied in second order. The line shapes were measured under experimental conditions that ensured the linearity of signal with electron beam current and gas pressure. The spectra were measured in the crossed beam mode, while the cross sections were measured in the static gas mode.

[11] The medium-resolution (0.6 Å full width at half maximum (FWHM)) overview of the FUV spectrum of electron impact-induced fluorescence of $e + O_2$ at 100 eV is shown in Figure 1. The spectrum consists of four multiplets centered near OI(1152 Å, 1218 Å, 1304 Å, 1356 Å), which we have previously identified from low-resolution studies [*Ajello*, 1971; *Ajello and Franklin*, 1985; *James et al.*, 1988]. In the medium-resolution spectrum we see the fine-structure transitions of the multiplets. To account for the relative spectral sensitivity of the 3 m spectrometer and channel electron multiplier detector at different wavelengths, the laboratory spectrum has been calibrated by methods established in our laboratory, involving electron excitation of the Rydberg states of H_2 [*Liu et al.*, 1995]. In addition to the calibration, the intensity of the OI(1356 Å) doublet structure has been corrected by a factor of ~175 in order to account for the diffusion out of the field of view (FOV) of long-lived OI $^5S^o$ atoms. This corrected value was obtained by comparing areas of 130.4 nm and 135.6 nm multiplets with cross section values for OI(130.4 nm) from *James et al.* [1988] and for OI(135.6 nm) from Paper 2. The weak 115.2 nm and 121.8 nm features were enhanced by a factor of 10 for visual purposes, and the spectrum was put on a relative scale. The absolute values of cross sections at 100 eV and their corresponding fine-structure transitions are given in Table 1. There are no molecular band systems in the FUV emission spectrum. The absence of band system emissions in the neighborhood of 10 eV transition energies can be explained by examining the known states of O_2 shown on the potential energy diagram of Figure 2. For example, the $B^1\Sigma^+_u$ state, which is the upper state of the strong Schumann-Runge system of O_2, with an electronic excitation energy of 6.2 eV, is almost completely predissociated. Figure 2 shows the electronic states of O_2 and O_2^+ as well as the first two or three dissociation limits for the OI(1152 Å, 1304 Å, 1356 Å) emissions from each of the dissociative excitation (near 14 eV) and dissociative ionization excitation (near 28 eV) processes. The theoretical and observed thresholds are summarized in Table 2.

Table 1. Emission Cross Sections of OI Transitions in the $O_2 + e$ (100 eV) Collision

Emission Line, Å	Cross Section, 10^{-18} cm^2
OI($^1D_2 \leftarrow {}^1D^o_2$) 1152.515	0.34
OI($^1S_0 \leftarrow {}^1P^o_1$) 1217.648	0.10
OI($g^3P_2 \leftarrow {}^3S^o_1$) 1302.168	1.58
OI($g^3P_1 \leftarrow {}^3S^o_1$) 1304.858	0.95
OI($g^3P_0 \leftarrow {}^3S^o_1$) 1306.029	0.30
OI($g^3P_2 \leftarrow {}^5S^o_2$) 1355.598	4.92
OI($g^3P_1 \leftarrow {}^5S^o_2$) 1358.512	1.48

[12] The electron impact-induced fluorescent line profiles of OI at 35 eV and 100 eV impact energies are shown in a series of spectra in Figures 3, 4, and 5 for 1152 Å, 1304 Å, and 1356 Å, respectively, along with the instrumental slit function of the spectrometer. Also shown are line profiles of the respective data, obtained by applying the filtering and symmetrization procedures explained in section 3. In this experiment the line profiles were measured at 90°, both to the electron and to the molecular beam axes.

3. Line Profile Analysis

[13] The measured line profile is the convolution of the true (emission) line profile and the instrumental slit function. Since the width of the instrumental slit function (FWHM = 27 mÅ in third order and FWHM = 32 mÅ in second order) is comparable to the observed emission line width (FWHM = 47 mÅ) for OI (1152 Å) at 100 eV, as a typical example, the instrumental function must be deconvoluted from the observed line profile. A fast Fourier transform (FFT) technique was used to recover the actual line profile [*Press et al.*, 1986]. Expressed mathematically, the measured line profile, $I(\lambda)$, is given by the convolution integral

$$I(\lambda) = \int T(\lambda')A(\lambda - \lambda')d\lambda', \quad (1)$$

where $T(\lambda')$ is the true line profile at wavelength λ' and $A(\lambda - \lambda')$ is the instrumental response function.

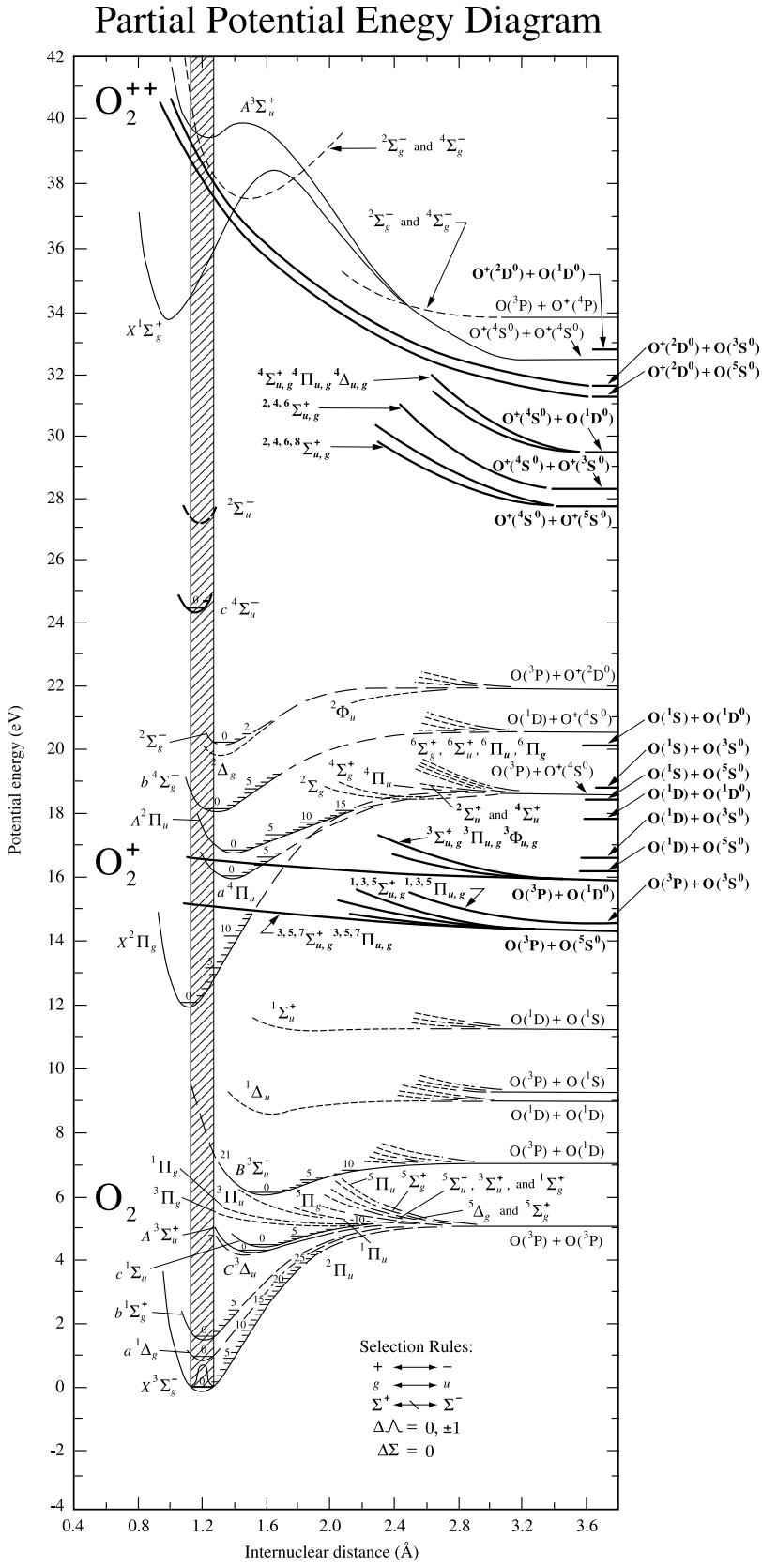

Figure 2. Partial potential energy diagram of O_2 adopted from *Krupenie* [1972]. The dissociation limits for the atomic oxygen products observed in this study are shown. Some of the O_2 states for the repulsive curves responsible for the dissociation process are identified, and the potential energy curves are sketched in the Franck-Condon region.

Table 2. Calculated and Observed Thresholds for OI(1152 Å, 1304 Å, 1356 Å)

States	Theory Appearance Threshold Potentials, eV	Observed Appearance Threshold Potentials, eV	Dissociating State
	OI(1152.2 Å)		
$O(g^3P) + O(^1D^o)$	15.9	15.9	$^3\Pi_u$
$O(^1D) + O(^1D^o)$	17.8		
$O(^1S) + O(^1D^o)$	20.1	~24	
$O^+(^4S^o) + O(^1D^o)$	29.5	~36	$^4\Sigma_u^+$, $^4\Pi_u$
$O^+(^2D^o) + O(^1D^o)$	32.8		$^2\Sigma_u^-$, $^2\Pi_u$
$O^+(^2P^o) + O(^1D^o)$	34.5		
	OI(1303.5 Å)		
$O(g^3P) + O(^3S^o)$	14.6	14.6	$^3\Pi_u$
$O(^1D) + O(^3S^o)$	16.6		
$O(^1S) + O(^3S^o)$	18.8	~23	
$O^+(^4S^o) + O(^3S^o)$	28.3		$^{2,4}\Sigma_u^+$ forbidden
$O^+(^2D^o) + O(^3S^o)$	31.6	~38	$^{2,4}\Pi_u$
$O^+(^2P^o) + O(^3S^o)$	34.5		
	OI(1355.6 Å)		
$O(g^3P) + O(^5S^o)$	14.3	14.3	$^3\Pi_u$
$O(^1D) + O(^5S^o)$	16.2	~18	
$O(^1S) + O(^5S^o)$	18.5		
$O^+(^4S^o) + O(^5S^o)$	27.9		$^{2,4}\Sigma_u^+$ forbidden
$O^+(^2D^o) + O(^5S^o)$	31.2	~38	$^{2,4}\Pi_u$
$O^+(^2P^o) + O(^5S^o)$	32.9		

[14] The instrumental response function is determined from the slit function shown in Figures 3, 6, and 9. The mathematical FFT technique has been fully explained in our previous studies [*Ajello et al.*, 1995a, 1995b]. We selected a step filter to remove high-frequency noise from FFTs of the measured signal, I_T, and of the instrumental response function, A_T. Then each data set (measured signal and instrumental slit function) was symmetrized around the central peak by taking two points equidistant from the peak and replacing them both with their average value. (The resulting line profile, in effect, appears to be shifted sideways by a fraction of the wavelength step used in the measurement and is otherwise almost indistinguishable from the initial line profile.)

[15] Then, the low-pass step filter, F_T, was applied to the ratio A_T/I_T to obtain the FFT of the true line profile, T_T. The low-pass step filter was modified by a Welch window [*Press et al.*, 1986] in order to eliminate spectral leakage into side lobes of the deconvoluted line profiles. The signal-to-noise (S/N) ratio is >50 for all line profiles with the exception of OI(135.6 nm), for which the S/N ratio was estimated to be equal to 10. The true line profile, $T(\lambda)$, and the measured line profile, $I(\lambda)$, at low energies, and the slit function are all approximately Gaussian in form. The root-sum-square of the FWHM of the true line shape and the slit function should approximately equal the FWHM of the measured profile. This is found to be the case within anywhere from 1 mÅ for the OI(115.2 nm) 35 eV line profile to 15 m for the OI(135.6 nm) 100 eV line profile.

[16] We show in Figure 4 the deconvoluted true line profiles, $T(\lambda)$, for 35 eV and 100 eV OI(1152 Å) transitions. The true line profiles have a FWHM of 23 ± 1 m and 42 ± 3 mÅ for the OI(1152 Å) line profiles at 35 and 100 eV, respectively. Line profile measurements for OI(1302 Å) at 25–35 eV electron impact energy revealed FWHM values of the convoluted line profile comparable to those of the instrumental slit functions. Thus low-energy measurements of the OI(1302 Å) line profile were not taken, and data are presented here only for 100 eV electron impact energy. Figure 7 shows the result of deconvolution of the 100 eV OI(1302 Å) line profile. For 100 eV energy a FWHM of the true line profile is 27 ± 8 m. Finally, the line profile for the OI(1356 Å) transition was measured with only 100 eV electron impact energy due to a very low intensity of the emission from long-lived metastable states of OI $^5S^o$ quintets at low (20–30 eV) impact energies. The 100 eV OI(1356 Å) deconvoluted true line profile is shown in Figure 10, and the FWHM of the true line profile was found to be 36 ± 7 m.

4. Kinetic Energy Distribution Analysis

[17] For each of the true line profiles in Figures 4, 7, and 10 the corresponding kinetic energy distribution of the fragments, $P(E)$, is given by

$$P(E) = k\frac{dT}{d\lambda}, \tag{2}$$

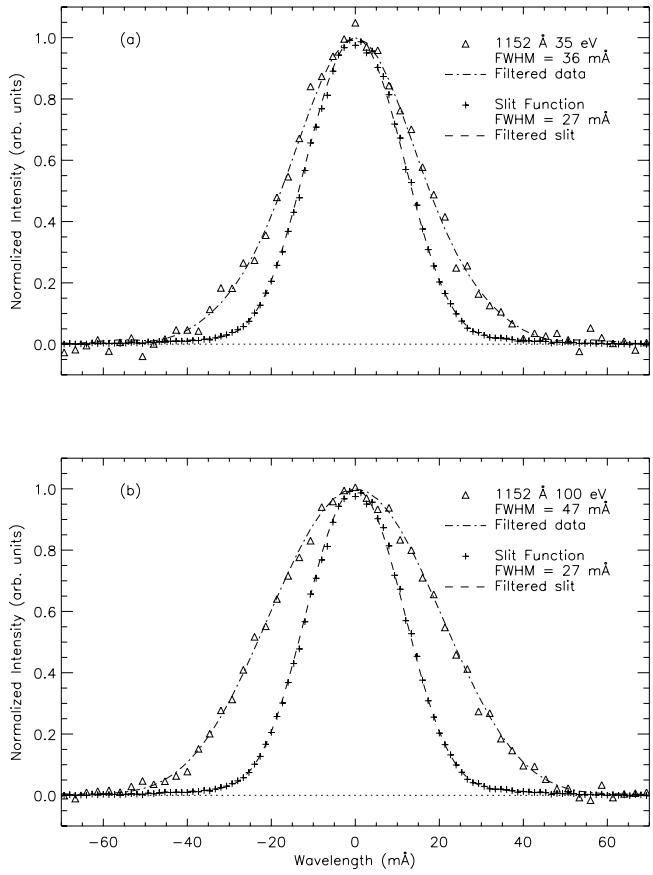

Figure 3. High-resolution experimental line profile spectrum of OI($^1D_2 \leftarrow ^1D_2^o$) at 1152.16 Å (measured data, triangles; filtered and symmetrized data, dash-dotted line) and the instrumental slit function (measured data, crosses; filtered and symmetrized data, dashed line) at 27 mÅ FWHM in third order at (a) 35 eV and (b) 100 eV impact energies. The step size was 2.667 mÅ channel^{-1}. The background pressure was 9×10^{-6} torr, with an electron beam current of ~200 μA.

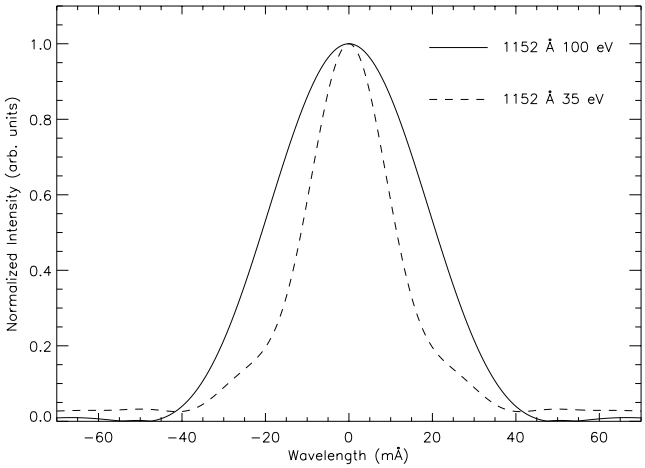

Figure 4. True line profile, $T(\lambda)$, of the 35 eV (dashed line) and 100eV (solid line) OI(1152 Å) transitions obtained from the measured profiles of Figure 3 using a fast Fourier transform (FFT) technique.

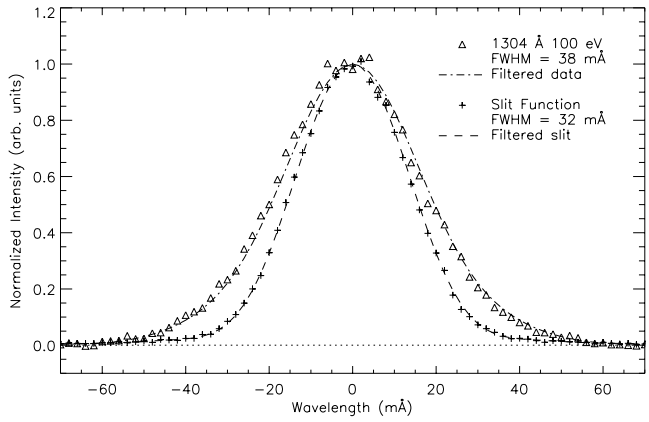

Figure 6. High-resolution experimental line profile spectrum of OI($g^3P_2 \leftarrow {}^3S_2^o$) at 1302.17 Å (measured data, triangles; filtered and symmetrized data, dash-dotted line) and the instrumental slit function (measured data, crosses; filtered and symmetrized data, dashed line) at 32 mÅ FWHM in second order at 100 eV impact energy. The step size was 2 mÅ channel^{-1}. The background pressure was 9×10^{-6} torr, with an electron beam current of $\sim$200 μA.

where k is a multiplicative constant [*Ogawa and Higo*, 1979, 1980; *Ogawa et al.*, 1992]. The expression is rigorous if the distribution function is isotropic.

[18] The normalized kinetic energy distribution of the OI $^1D_2^o$ fragments is shown in Figure 5. The fragment distribution of OI $^1D_2^o$ for 35 eV electron impact energy has a FWHM of 1.6 ± 0.2 eV, with a peak energy of 0.45 ± 0.04 eV and a mean energy of 2.4 ± 0.2 eV. For 100 eV electron impact energy the fragment distribution is broader, with a FWHM of 6.6 ± 0.9 eV, with a peak energy of 2.1 ± 0.3 eV, and with a mean energy of fragments of 4.0 ± 0.6 eV. The errors for the peak, FWHM, and mean values of the kinetic energy distribution of fragments were derived from the error estimates of the FWHM of the deconvoluted true line profiles presented in section 3.

[19] The normalized kinetic energy distribution of the OI $^3S_1^o$ fragments is shown in Figure 8. The fragment distribution of OI $^3S_1^o$ has a FWHM of 2 ± 1 eV, with a peak of 0.6 ± 0.3 eV and a mean energy of 2.5 ± 1.2 eV for 100 eV electron impact energy.

[20] Figure 11 shows the normalized kinetic energy distribution of OI $^5S_2^o$ fragments. Since oxygen atoms in the $^5S_2^o$ state have a long radiative lifetime ($\sim$180 μs), not all of these atoms will radiate in the FOV of the spectrometer as they drift away from the interaction region. The lower the velocity of such oxygen atoms, the higher the probability that the atoms will radiate while still in the FOV of the spectrometer. This skews the energy distribution toward lower energies, giving the appearance that slower fragments dominate the energy distribution. Therefore the energy distribution had to be adjusted.

[21] To find a correction factor for the distribution at any given energy, we considered a hypothetical model in which all atoms drift away from the interaction region with a constant velocity uniformly in all directions. The geometry

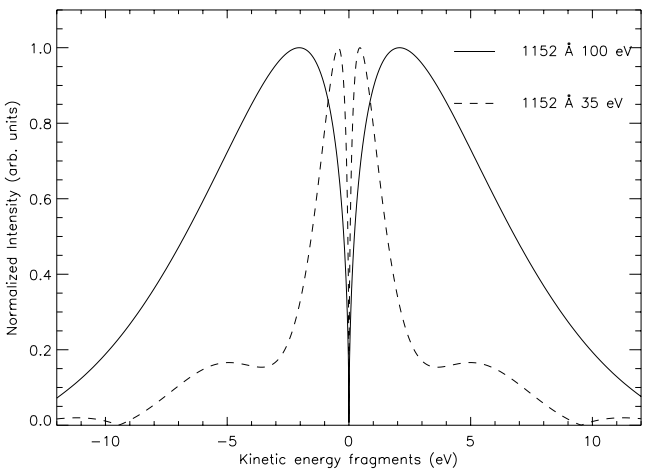

Figure 5. Kinetic energy distribution, $P(E)$, of OI(^1D) atoms at 35 eV (dashed line) and 100 eV (solid line) electron energy from dissociative excitation of O_2.

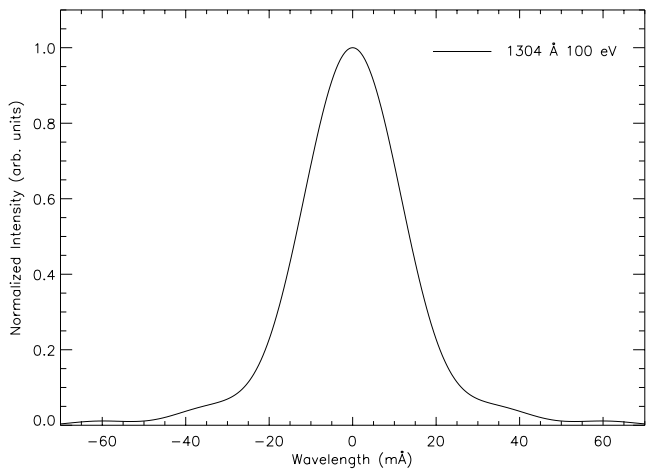

Figure 7. True line profile, $T(\lambda)$, of the 100 eV OI(1304 Å) transition obtained from the measured profile of Figure 6 using a FFT technique.

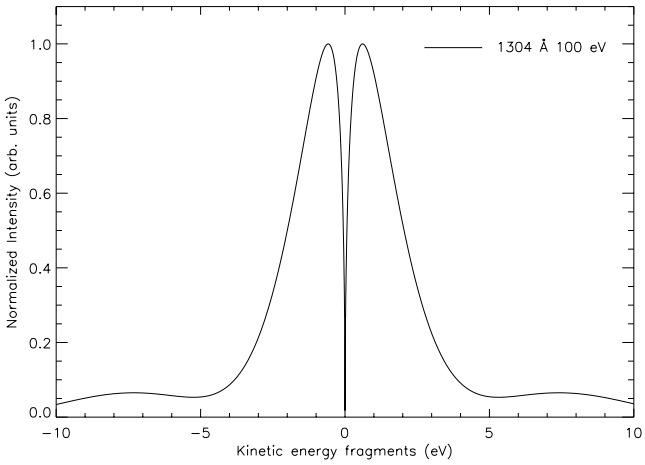

Figure 8. Kinetic energy distribution, $P(E)$, of OI($^3S^o$) atoms at 100 eV electron energy from dissociative excitation of O_2.

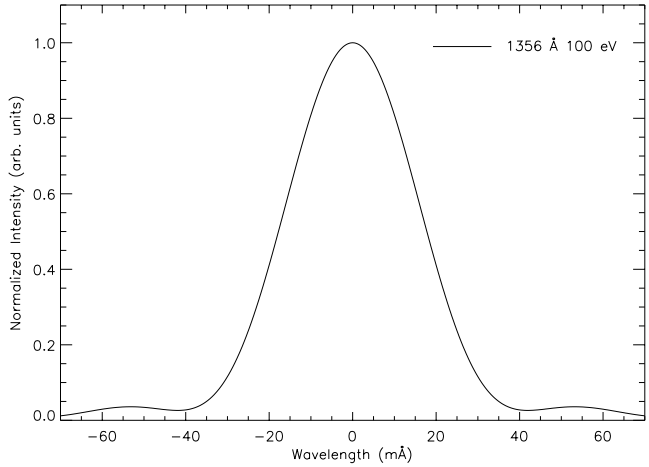

Figure 10. True line profile, $T(\lambda)$, of the 100 eV OI(1356 Å) transition obtained from the measured profile of Figure 9 using a FFT technique.

of a system, consisting of the collision chamber, entrance slit, and spectrometer, defines a volume from which the OI(135.6 nm) glow will be seen at the location of the diffraction grating. The volume has the shape of a wedge, with the tip of the wedge along the entrance slit of the spectrometer (4 mm × 15–20 μ) and with a base of 4.15 × 11 mm at the location of the back mirror. The back mirror is used to reflect the radiation toward the entrance slit of the spectrometer and is located at a distance of 20.64 cm from the interaction region on the side opposite the entrance slit. The entrance slit is located at a distance of 11.05 cm from the interaction region. Inside this volume the atoms will drift in all directions, ranging from the direction with the shortest possible distance, d_{min}, before escaping the volume to the longest distance, d_{max}, toward the back reflecting mirror.

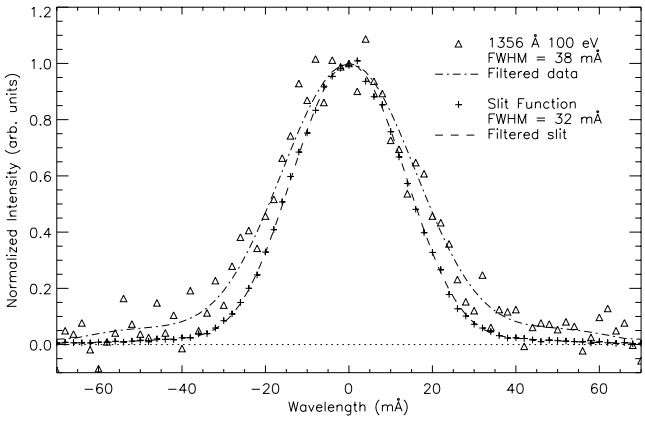

Figure 9. High-resolution experimental line profile spectrum of OI($g^3P_2 \leftarrow {}^5S_2^o$) at 1355.60 Å (measured data, triangles; filtered and symmetrized data, dash-dotted line) and the instrumental slit function (measured data, crosses; filtered and symmetrized data, dashed line) at 32 mÅ FWHM in third order at 100 eV impact energy. The step size was 2 mÅ channel^{-1}. The background pressure was 9×10^{-6} torr, with an electron beam current of ~200 μA.

[22] For each distance r from this range we use the model of *Ajello* [1970] to calculate the fraction of atoms that radiates while traversing the distance. As a first step in model calculations, the fraction $f(r)$, where $d_{min} \leq r \leq d_{max}$, is calculated as a ratio of the number of atoms radiating while traversing distance 0 to r to the total number of atoms radiating while traversing distance r from 0 to ∞. The next step in the model calculations is to obtain the average, $\overline{f(r)}$, of the fractions of atoms radiating inside the volume by summing fractions at distances r and $f(r)$, weighted with a distribution of r's inside the volume. Thus the correction factor was obtained for each energy of the fragments and was used to adjust the energy distribution. For 100 eV impact energy the corrected fragment distribution has a FWHM value of 3.7 ± 1.4 eV, with a peak of 1.3 ± 0.5 eV and a mean of 2.4 ± 1.0 eV.

5. Discussion

[23] Figures 12, 13, and 14 show the threshold behavior (up to 50 eV) of the absolute cross sections of OI(115.2 nm),

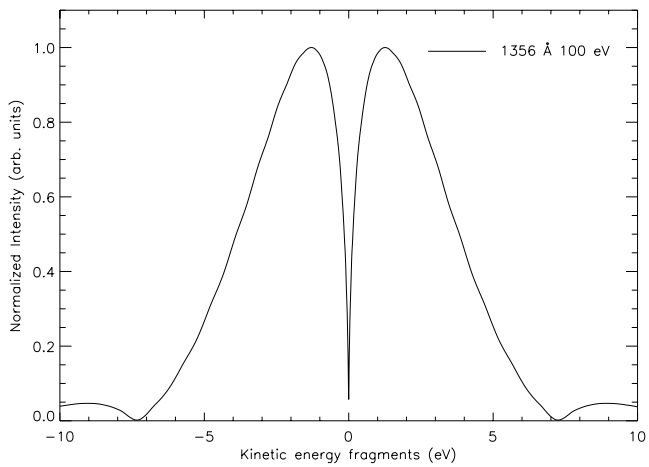

Figure 11. Kinetic energy distribution, $P(E)$, of OI($^5S^o$) atoms at 100 eV electron energy from dissociative excitation of O_2.

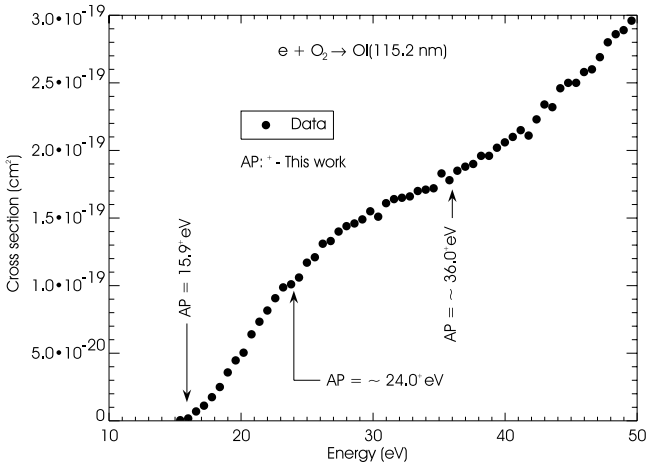

Figure 12. Absolute cross section of OI($^1D \leftarrow {}^1D^o$) at 115.2 nm from threshold to 50 eV at a resolution of 0.6 nm.

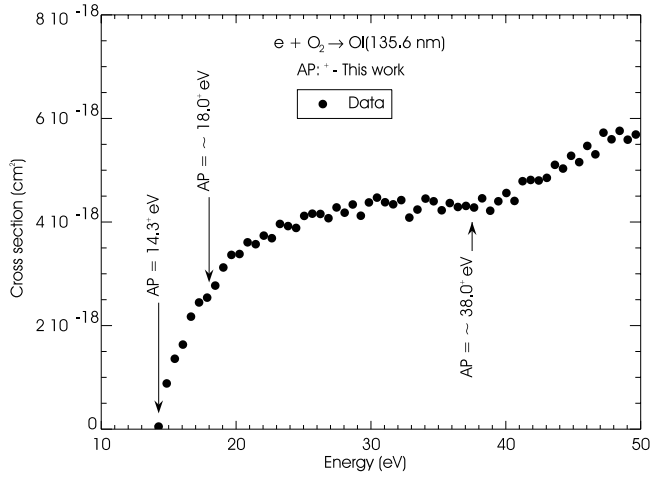

Figure 14. Absolute cross section of OI($g^3P \leftarrow {}^5S^o$) at 135.6 nm from threshold to 50 eV at a resolution of 0.6 nm.

OI(130.4 nm), and OI(135.6 nm) emissions, respectively. The measured cross sections shown are part of the full cross section measurements (up to 600 eV) presented in Paper 2. The optical excitation functions were measured in static gas mode with the resolution of the spectrometer set to 0.6 nm. The normalization details of optical excitation functions are presented in Paper 2. The appearance threshold potentials (AP) are identified in Figures 12, 13, and 14. The AP with values below ~25 eV are due to dissociative excitation of O_2 (see Figure 2 and Table 2), and AP with values >25 eV are due to dissociative ionization and excitation of O_2.

[24] At 35 eV electron impact energy the OI(115.2 nm) emission is from the dissociation of excited O_2 into fragments shown in the first three rows for transition OI(115.2 nm) in Table 2. For the product states shown in the first row, OI(g^3P) + OI($^1D^o$), the energy level of the separated system together with the sketch of the energy level at a smaller internuclear distance crossing the Franck-Condon region is shown in Figure 2. For product states from the second and third rows, only the energy levels of the separated system are shown. The AP of the threshold near 24 eV in Figure 12 most likely appears from the product states OI(^1S) + OI($^1D^o$), which have a theoretical threshold of 20.1 eV. This is also supported by the fact that the peak kinetic energy distribution of OI $^1D_2^o$ at 35 eV is equal to 0.45 eV. At 100 eV, faster fragments come from dissociation of states of OII near 28–35 eV shown in the last three rows for the transition of OI(115.2 nm) in Table 2. These states cross the Franck-Condon region at 4–5 eV higher than the asymptotic limit of 29.46 eV for molecular ion states.

[25] At 100 eV electron impact energy for transition OI(130.4 nm) in Table 2 the fast fragments come from the dissociation of O_2^+ molecular ion states, which asymptotically approach energy levels at 28.22 eV and above. The peak energy of oxygen fragments in the $^3S_1^o$ state, which is 0.6 eV, would suggest that emission comes from the dissociation of O_2^+ into fragments shown in the last row for the transition OI(130.4 nm) in Table 2.

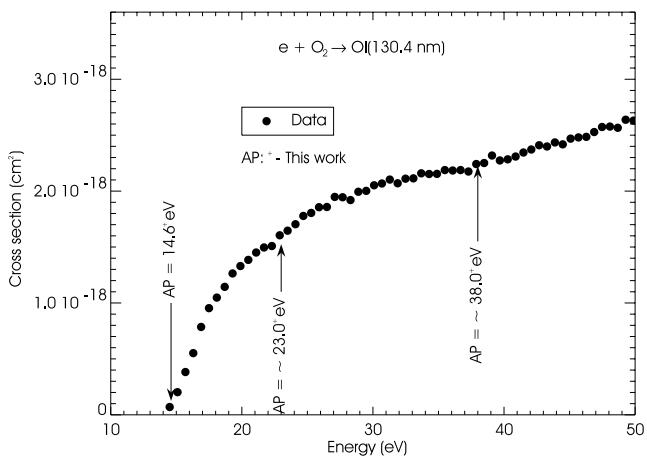

Figure 13. Absolute cross section of OI($g^3P \leftarrow {}^3S^o$) at 130.4 nm from threshold to 50 eV at a resolution of 0.6 nm.

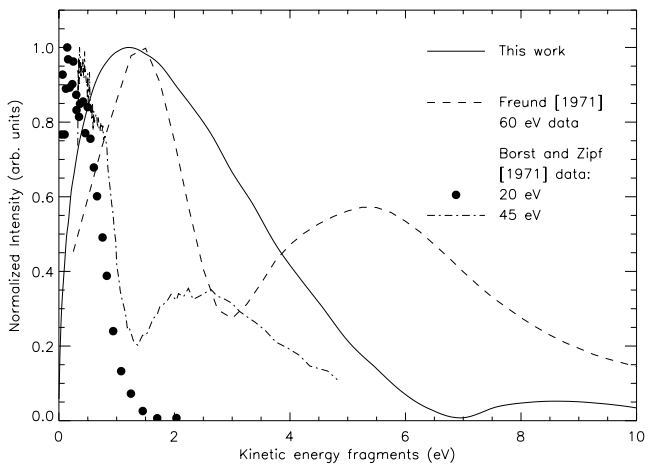

Figure 15. Relative comparison of the kinetic energy distribution function of oxygen atom fragments in OI($g^3P \leftarrow {}^5S^o$) at 135.6 nm: this work at 100 eV impact electron energy (solid line) and *Freund* [1971] data at 60 eV electron impact energy (dashed line); *Borst and Zipf* [1971] data at 20 eV electron impact energy (circles); *Borst and Zipf* [1971] data at 45 eV electron impact energy (dash-dotted line).

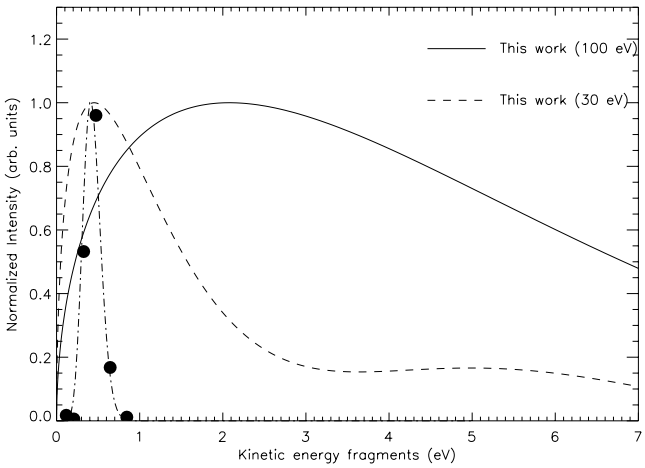

Figure 16. Relative comparison of the kinetic energy distribution function of oxygen atom fragments in OI($^1D \leftarrow {}^1D^o$) at 115.2 nm: this work at E = 100 eV (solid line); this work at E = 30 eV (dashed line); the data of *Matsumi et al.* [1994] (circles); and the Gaussian fit of filled dots from *Matsumi et al.* [1994] (dash-dotted line).

[26] For the OI(135.6 nm) transition the asymptotical limits of the dissociating states are at 27.84 eV and above. One limit, at 31.17 eV, is shown crossing the Franck-Condon region near 38 eV in Figure 2.

[27] *Freund* [1971] measured the translational energy of the metastable atoms in the $3s^5S^o$ state after the dissociation of O_2 by low-energy electrons. We show in Figure 15 the relative comparison of kinetic energy distributions of metastable fragments measured in this work (solid line) and by *Freund* [1971] (dashed line). *Freund*'s [1971] data were obtained by measuring the time-of-flight distribution of the dissociation fragments registered by the Auger detector. We compare our results to those of *Freund* [1971] at 60 eV electron impact energy. The first peak at 1.5 eV in *Freund*'s [1971] data is what he refers to as peak A1, the result of the direct dissociation of the $^3\Pi_u$ state into the sum of OI($^5S^o$) + OI(g^3P) (see Figure 2). The second peak in *Freund*'s [1971] data he refers to as two peaks, A2 and A3, which *Freund* [1971] speculates are the results from Rydberg state dissociation processes, which correspond to the predissociation of $c^4\Sigma_u^-$ and $^2\Pi_u$ III core ions. The state $c^4\Sigma_u^-$ is known from optical emission spectra and is shown in Figure 2. The state $^2\Pi_u$ III is not shown in Figure 2, but it appears at 22–23 eV in the Frank-Condon region in Figure 11 of *Freund* [1971]. These states, according to *Freund* [1971], are predissociated into high-quintet Rydberg atoms with ground state oxygen ion cores ($^4S^o$), from which they cascade to the lowest quintet state, $^5S^o$.

[28] At 60 eV impact energy, there should also be excited states mixed in from the higher-energy level region near 28–38 eV. *Freund* [1971] did not mention these states in the discussion of his results. Our measurement of the excitation function at 135.6 nm shows that thresholds appear at that level, indicating that at higher impact energies we have a mixture of quintet states dissociated from O_2 and O_2^+ states.

[29] We show in Figure 15 the results of *Borst and Zipf* [1971], who also measured the translational energy spectra of metastable oxygen atoms produced by electron impact dissociation of O_2. *Borst and Zipf* [1971] presented the results obtained with electron impact energies up to 60 eV. We present in Figure 15 the data for two impact energies, 20 eV and 45 eV. The data at 20 eV electron impact energy are presented as they were presented by *Borst and Zipf* [1971], and the data at 45 eV are the time-of-flight distribution converted to an energy spectrum as outlined by *Borst and Zipf* [1971]. The data of *Borst and Zipf* [1971] resemble those of *Freund* [1971], although on a different energy scale. Aside from the energy scale, the qualitative behavior of the *Borst and Zipf* [1971] data agrees with that of the present work and with the *Freund* [1971] data.

[30] We show in Figure 16 the relative kinetic energy distribution functions of oxygen atom fragments for OI($^1D \leftarrow {}^1D^o$) at 115.2 nm for a positive velocity of the fragments. In Figure 16 we also show the kinetic energy distribution function from the work of *Matsumi et al.* [1994]. *Matsumi et al.* [1994] studied the velocity relaxation of hot OI ^{1}D atoms by collisions with rare gases, N_2, and O_2. As the initial part of their work, they measured the nascent speed distribution of the OI ^{1}D atoms generated in the 157 nm photodissociation of O_2. The energy of the laser photon (7.9 eV) corresponded to the energy of excitation of ground state oxygen molecules to the $B^3\Sigma_u^-$ state above the asymptotic level of the dissociating products OI g^3P and OI ^1D (see Figure 2). These two atomic states were the sole primary photodissociation products of O_2. The excitation energy excess above the dissociation limit resulted in the narrow kinetic energy distribution, centered at 4.1 $\times$ 10^4 J mol^{-1}, or 0.42 eV, as seen in Figure 16. Solid circles in Figure 16 are the measured nascent speed distributions of *Matsumi et al.* [1994] converted from velocity dependence to energy dependence, and the dash-dotted line is the Gaussian fit of the speed distribution as a function of velocity.

[31] The results of this work show a much broader distribution of kinetic energy fragments of O_2 in collisions with 30 eV and 100 eV electrons, as shown in Figure 16. The present work studied the speed distribution of the

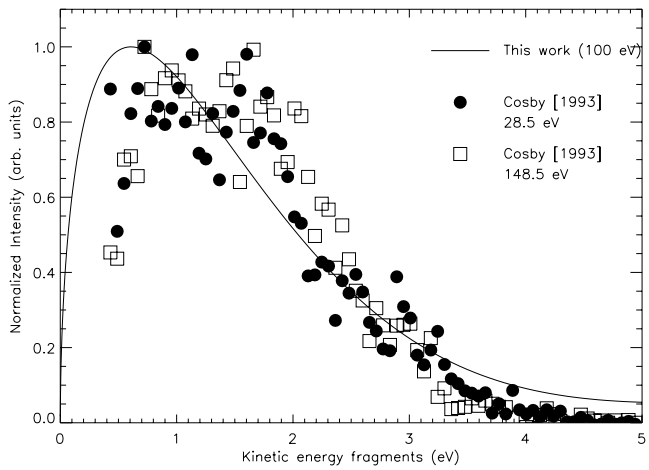

Figure 17. Relative comparison of the kinetic energy distribution function of oxygen atom fragments in OI($g^3P \leftarrow {}^3S^o$) at 130.2 nm: this work at 100 eV electron impact energy (solid line); and the data of *Cosby* [1993] at 28.5 eV (circles) and 148.5 eV (squares) electron impact energies.

oxygen fragments resulting from the dissociation of molecular states in the 14–20 eV and 28–38 eV regions above the ground state energy of O_2 (see Figure 2). At 30 eV impact energy the resulting fragments primarily originated from molecular states near 14–20 eV above the ground level, which asymptotically evolve into two atomic states with one of the products in the $3s^1D^o$ state of oxygen. At 100 eV impact energy the resulting fragments are from the states of both O^2 and O_2^+, the latter from near 28–38 eV above the ground level of O_2. In this case the resulting kinetic energy fragment distribution is broader and shifted toward higher kinetic energies as compared to 30 eV impact energy. Thus, whereas *Matsumi et al.* [1994] studied the kinetic energy distribution of the lower state (^{1} D) of the OI($^1D \leftarrow {}^1D^o$) transition at 115.2 nm, this work concentrated on the kinetic energy distribution of the upper $^1D^o$ state.

[32] *Cosby* [1993] studied the electron impact dissociation of O_2 and electron energies between 13.5 and 198.5 eV. The author observed translational energy releases in the O_2 dissociation, which are consistent with the production of OI(^{1} D) + OI(g^3P) fragments following electron impact excitation to the $B^3\Sigma_u^-$, $B'^3\Sigma_u^-$, and $2^3\Pi_u$ states and the production of OI(g^3P) + OI(g^3P) fragments from excitation to the (unresolved) $c^1\Sigma_u^-$, $A'^3\Delta_u$, and $A^3\Sigma_u^+$ states (see Figure 2, where some of these states are shown). The results of the work of *Cosby* [1993] for electron beam energies of 28.5 eV and 148.5 eV are shown in Figure 17, together with the results of the present work for kinetic energy distributions of oxygen fragments in the $3s^3S^o$ state observed in the OI($g^3P \leftarrow {}^3S^o$) transition at 130.2 nm. Again, as in the case of comparing the present work to the work of *Matsumi et al.* [1994], the results of the present work differ from those of *Cosby* [1993] in that in our work we observed the kinetic energy distributions of the upper states ($^1D^o$, $^3S^o$, and $^5S^o$) in transitions OI($^1D \leftarrow {}^1D^o$), OI($g^3P \leftarrow {}^3S^o$), and OI($g^3P \leftarrow {}^5S^o$). The knowledge of the kinetic energy distribution of these excited fragments enables us to estimate the behavior of molecular states which intersect the Frank-Condon region in the range of ~14 eV and above. In the cases of *Cosby* [1993] and *Matsumi et al.* [1994], their results led to the estimation of the behavior of molecular states in the range <14 eV.

[33] **Acknowledgments.** The research described in this paper was carried out at the Jet Propulsion Laboratory, California Institute of Technology, and was sponsored by the U.S. Air Force Office of Scientific Research (AFOSR), the Aeronomy Program of the National Science Foundation (ATM-9320589), the Planetary Atmospheres Program Office, Space Astrophysics Research Program Office, and the Space Physics Program Office of the National Aeronautics and Space Administration. One of us (OPM) is supported by the National Research Council through a Resident Research Associateship at the Jet Propulsion Laboratory, California Institute of Technology.

References

Ajello, J. M., Emission cross sections of N_2 in the vacuum ultraviolet by electron impact, *J. Chem. Phys.*, *53*, 1156–1165, 1970.

Ajello, J. M., Dissociative excitation of O_2 in the vacuum ultraviolet by electron impact, *J. Chem. Phys.*, *55*, 3156–3157, 1971.

Ajello, J. M., and M. Ciocca, Fast nitrogen atoms from dissociative excitation of N_2 by electron impact, *J. Geophys. Res.*, *101*, 18,953–18,960, 1996.

Ajello, J. M., and B. Franklin, A study of the extreme ultraviolet spectrum of O_2 by electron impact, *J. Chem. Phys.*, *82*, 2519–2528, 1985.

Ajello, J. M., G. K. James, I. Kanik, and B. O. Franklin, The complete UV spectrum of SO_2 by electron impact: 1. The vacuum ultraviolet spectrum, *J. Geophys. Res.*, *97*, 10,473–10,500, 1992a.

Ajello, J. M., G. K. James, and I. Kanik, The complete UV spectrum of SO_2 by electron impact: 2. The middle ultraviolet spectrum, *J. Geophys. Res.*, *97*, 10,501–10,512, 1992b.

Ajello, J. M., S. M. Ahmed, I. Kanik, and R. Multari, Kinetic energy distribution of H(2*p*) atoms from dissociative excitation of H_2, *Phys. Rev. Lett.*, *75*, 3261–3264, 1995a.

Ajello, J. M., I. Kanik, S. M. Ahmed, and J. T. Clarke, Line profile of H Lyman α from dissociative excitation of H_2 with application to Jupiter, *J. Geophys. Res.*, *100*, 26,411–26,420, 1995b.

Ajello, J. M., S. M. Ahmed, and X. Liu, Line profile of H Lyman-β emission from dissociative excitation of H_2, *Phys. Rev. A*, *53*, 2303–2308, 1996.

Beegle, L. W., J. M. Ajello, G. K. James, D. Dziczek, and M. Alvarez, High resolution emission spectroscopy of the $A^1\Pi$-$X^1\Sigma^+$ fourth positive band system of CO excited by electron impact, *Astron. Astrophys.*, *347*, 375–390, 1999.

Borst, W. L., and E. C. Zipf, Energy spectra of metastable oxygen atoms produced by electron-impact dissociation of O_2, *Phys. Rev. A*, *4*, 153–161, 1971.

Ciocca, M., J. M. Ajello, X. Liu, and J. Maki, Kinetic-energy distribution of D(2*p*) atoms from analysis of the D Lyman-α line profile, *Phys. Rev. A*, *56*, 1929–1937, 1997.

Clarke, J. T., J. Ajello, J. Luhmann, N. Schneider, and I. Kanik, Hubble Space Telescope UV spectral observations of Io passing into eclipse, *J. Geophys. Res.*, *99*, 8387–8402, 1994.

Cosby, P. C., Electron-impact dissociation of oxygen, *J. Chem. Phys.*, *98*, 9560–9569, 1993.

Feldman, P. D., M. A. McGrath, D. F. Strobel, H. W. Moos, K. D. Retherford, and B. C. Wolven, HST/STIS ultraviolet imaging of polar aurora on Ganymede, *Astrophys. J.*, *535*, 1085–1090, 2000.

Freund, R. S., Dissociation by electron impact of oxygen into metastable quintet and long-lived high-Rydberg atoms, *J. Chem. Phys.*, *54*, 3125–3141, 1971.

Hall, D. T., D. F. Strobel, P. D. Feldman, M. A. McGrath, and H. A. Weaver, Detection of an oxygen atmosphere on Jupiter's moon Europa, *Nature*, *373*, 677–679, 1995.

Hall, D. T., P. D. Feldman, M. A. McGrath, and D. F. Strobel, The far-ultraviolet oxygen airglow of Europa and Ganymede, *Astrophys. J.*, *499*, 475–481, 1998.

James, G. K., J. M. Ajello, D. E. Shemansky, B. Franklin, D. Siskind, and T. G. Slanger, An investigation of the second negative system of O_2^+ by electron impact, *J. Geophys. Res.*, *93*, 9893–9902, 1988.

Kanik, I., C. Noren, O. P. Makarov, P. Vattipalle, J. M. Ajello, and D. E. Shemansky, Electron impact dissociative excitation of O2: 2. Absolute emission cross sections of the OI(130.4 nm) and OI(135.6 nm) lines, *J. Geophys. Res.*, *108*, doi:10.1029/2000JE001423, in press, 2003.

Krupenie, P. H., The spectrum of molecular oxygen, *J. Phys. Chem. Ref. Data*, *1*, 423–534, 1972.

Kumar, S., and D. M. Hunten, The atmospheres of Io and other satellites, in *Satellites of Jupiter*, edited by D. Morrison, pp. 782–806, Univ. of Ariz. Press, Tucson, 1982.

Liu, X., S. M. Ahmed, R. A. Multari, G. K. James, and J. M. Ajello, High-resolution electron-impact study of the far-ultraviolet emission spectrum of molecular hydrogen, *Astrophys. J.*, *101*, 375–399, 1995.

Matsumi, Y., S. M. Shamsuddin, Y. Sato, and M. Kawasaki, Velocity relaxation of hot O(^1D) atoms by collisions with rare gases, N_2, and O_2, *J. Chem. Phys.*, *101*, 9610–9618, 1994.

Ogawa, T., and M. Higo, Analysis of the translational energy distribution of H^* produced in the e-H_2 collision, *Chem. Phys. Lett.*, *65*, 610–612, 1979.

Ogawa, T., and M. Higo, Translational energy distribution and production mechanism of excited hydrogen atoms produced by controlled electron impact on H2, *Chem. Phys.*, *52*, 55–64, 1980.

Ogawa, T., S. Ihara, and K. Nakashima, Fano plots for the slow and fast groups of excited hydrogen atoms produced in e-H_2 collisions, *Chem. Phys.*, *161*, 509–513, 1992.

Press, W. H., B. P. Flannery, S. A. Teukolsky, and W. T. Vetterling, *Numerical Recipes—The Art of Scientific Computing*, 818 pp., Cambridge Univ. Press, New York, 1986.

Torr, M. R., et al., A far ultraviolet imager for the international solar-terrestrial physics mission, *Space Sci. Rev.*, *71*, 329–383, 1995.

Wiese, W. L., J. R. Fuhr, and T. M. Deters, *Atomic Transition Probabilities of Carbon, Nitrogen, and Oxygen: A Critical Data Compilation*, 522 pp., Am. Chem. Soc., Woodbury, New York, 1996.

Yung, Y. L., and M. B. McElroy, Stability of an oxygen atmosphere on Ganymede, *Icarus*, *30*, 97–103, 1977.

J. M. Ajello, I. Kanik, and O. P. Makarov, Jet Propulsion Laboratory, California Institute of Technology, 4800 Oak Grove Drive, Pasadena, CA 91109, USA. (Oleg.Makarov@uconn.edu; ikanik@mail1.jpl.nasa.gov; jajello@lively.jpl.nasa.gov)